
Titanium Sapphire Lasers

K.F. Wall and A. Sanchez

■ In 1982 researchers at Lincoln Laboratory operated a tunable laser based on Ti:Al₂O₃ for the first time. A wide variety of developments in Ti:Al₂O₃ laser technology then followed the advances in crystal growth that occurred during the mid-1980s. Since that time researchers have demonstrated high efficiency, wide tunability, frequency-stable continuous-wave operation, and generation of very short pulses (<10⁻¹³ sec) with Ti:Al₂O₃ lasers. Ti:Al₂O₃ lasers are now commercially available and are a valuable research tool found in many laboratories. This article reviews some of the developments in Ti:Al₂O₃ lasers and focuses on contributions made at Lincoln Laboratory.

IN 1960 T.H. MAIMAN DEMONSTRATED the operation of the first optical maser, or laser [1]. Maiman's experiments used a crystal of synthetically grown ruby, or sapphire (Al₂O₃) doped with a small amount of chromium. Twenty-two years later P.F. Moulton demonstrated a widely tunable laser at Lincoln Laboratory by incorporating titanium instead of chromium as an impurity into sapphire [2]. Titanium-doped sapphire, or Ti:Al₂O₃, has the largest tuning range of any laser (from 660 to 1180 nm or, equivalently, from 15,200 to 8500 cm⁻¹). The corresponding fractional tuning range is 57%. See the box entitled "Tunable Lasers" for other examples of tunable lasers.

The Ti:Al₂O₃ crystals used in the initial experiments exhibited significant scattering and an unidentified absorption at the laser wavelength [3]. These losses affected the efficiency of the laser, and only pulsed operation was possible. Further advances in the development of the Ti:Al₂O₃ laser required higher-quality laser crystals. Room-temperature continuous-wave operation, first reported in 1986 [4, 5], resulted from the growth of Ti:Al₂O₃ crystals with significantly smaller losses [6]. As high-quality crystals became commercially available, a series of commercial lasers based upon Ti:Al₂O₃ appeared in 1988. Today Ti:Al₂O₃ lasers are used for a wide variety of applications in the laboratory.

Sapphire is an ideal host crystal in both the ruby and the Ti:Al₂O₃ laser. It is transparent from the ultraviolet to the infrared; also, it is nonhygroscopic and very hard (it has a hardness of 9 on the Mohs scale, compared to 10 for diamond), which is necessary for producing good optical-quality surfaces that are not easily scratched. The

thermal conductivity of sapphire, which is one-tenth that of copper at room temperature and comparable to that of copper at 80 K, is high compared to other laser hosts. The excellent mechanical, thermal, and optical properties of Ti:Al₂O₃ allow laser designs to be scaled to high average powers. A large number of tunable lasers, including Ti:Al₂O₃, have large efficiencies; most of the pump photons stimulate the emission of photons at the laser wavelength. For Ti:Al₂O₃ the overall power conversion efficiency can exceed 50% [7]. The generation of the appropriate pump photons, however, is often the major technical challenge.

Ni:MgF₂, the first tunable laser of any type, is a solid state laser that was demonstrated in 1964 [8]; dye lasers, which are also tunable, appeared in 1966 [9, 10]. In 1979 the demonstration of the Cr³⁺:BeAl₂O₄ (Alexandrite) laser [11], which operates at room temperature, led to renewed interest in tunable solid state lasers. Today dozens of tunable solid state lasers exist. Figure 1 is a representative partial list of the many tunable solid state lasers currently available.

The center frequency and tuning range of each laser depend on the active, or lasing, ion as well as the crystal host into which the ion is incorporated as an impurity. In the transition metal ions with an incomplete 3d shell (such as Cr³⁺, Ti³⁺, Co²⁺, Ni²⁺, and V²⁺), the lasing transition is between crystal-field-split energy levels of the ion; in a free ion these levels are degenerate (or have the same energy). In the tunable short-wavelength Ce³⁺ laser centered on 300 nm, lasing results from 4f to 5d transitions involving two different electron shells; the 4f electron when excited to the outer 5d electron shell is

TUNABLE LASERS

IN THIS ARTICLE we refer to a *tunable* laser as one whose frequency can be changed in a continuous manner over a large fraction (more than 5%) of its central frequency. This definition eliminates lasers such as argon-ion, krypton-ion, and helium-neon lasers that can lase at a number of specific frequencies but are not continuously tunable from one frequency to another. Narrowband continuously tunable radiation is desirable in a variety of spectroscopic techniques such as remote sensing, or for an agile-beam coherent laser radar system as described in this work. A broad bandwidth is desirable for the production of short pulses that have a variety of uses in spectroscopy.

A variety of lasers are tunable over an appreciable fraction of their central frequency. The most common tunable lasers are the organic dye lasers. A dye laser consists of an organic dye (such as a polymethine, xanthene, or coumarin dye) in a liquid solvent or host. A typical dye laser such as Rhodamine 6G can be tuned from 570 to 610 nm; other dyes have laser bandwidths that cover portions of the spectrum from the ultraviolet to the infrared. In a $\text{Ti}:\text{Al}_2\text{O}_3$ laser the laser transition is between two electronic levels of a single Ti^{3+} ion, and in dye lasers the laser transition is from one molecular electronic level to another. The broadening of the absorption and

luminescence bands is caused by the multitude of rotational levels associated with each molecular electronic level. Undesirable characteristics of dye lasers are toxicity of the dyes and solvents, degradation of the dyes with time, and amplitude noise in the laser output (because the dyes are flowed to reduce thermal loads).

Another class of tunable solid state lasers are the alkali-halide color-center lasers. A color center is a crystal defect in which an electron becomes trapped. For example, an F color center consists of an electron trapped at an anion vacancy of the crystal lattice. The excitations of the trapped electron strongly couple to the phonons of the lattice and give rise to broad absorption and emission bands. Color-center lasers can span the wavelength range from 800 nm, where organic dye lasers are of limited usefulness, to $4\ \mu\text{m}$. Color-center lasers have many drawbacks; one is that in many alkali-halide crystals the color centers are not stable at room temperature and will degrade on the time scale of a day. Color-center lasers doped with Tl^+ (tunable from 1.45 to $1.75\ \mu\text{m}$ and 2.3 to $3.45\ \mu\text{m}$), which have recently become commercially available, have solved the stability problem [1]. Cryogenic temperatures are necessary for the stability of many color-center lasers, and low temperatures are necessary for

efficient operation because the lifetime of the upper laser level decreases according to $1/T$, where T is the temperature. In addition, since alkali-halide crystals are hygroscopic, they must be contained in a cell.

Figure 1 summarizes other examples of tunable solid state lasers. $\text{Ni}^{2+}:\text{MgF}_2$ was actually the first tunable laser of any type [2]; an analog to it ($\text{Co}^{2+}:\text{MgF}_2$) interests the medical community because its tuning range overlaps strong absorption bands in water (of which the human body is primarily composed). Cr can be doped into a variety of materials and in many cases form tunable lasers (such as forsterite or alexandrite). Titanium-doped chrysoberyl is a second example of a tunable laser based upon Ti^{3+} [3]. Again, it should be pointed out that $\text{Ti}:\text{Al}_2\text{O}_3$ is the champion in terms of tuning range.

References

1. T.T. Basiev, S.B. Mirou, and V.V. Osiko, "Room-Temperature Color Center Lasers," *IEEE J. Quantum Electron.* **24**, 1052 (1988).
2. L.F. Johnson, R.E. Dietz, and H.J. Guggenheim, "Optical Maser Oscillation from Ni^{2+} in MgF_2 Involving Simultaneous Emission of Phonons," *Phys. Rev. Lett.* **11**, 318 (1963).
3. A.I. Alimpiev, G.V. Bukin, V.N. Matrosov, E.V. Pestryakov, V.P. Solntsev, V.I. Trunov, E.G. Tsvetkov, and V.P. Chebotaev, "Tunable $\text{BeAl}_2\text{O}_4:\text{Ti}^{3+}$ Laser," *Sov. J. Quantum Electron.* **16**, 579 (1986).

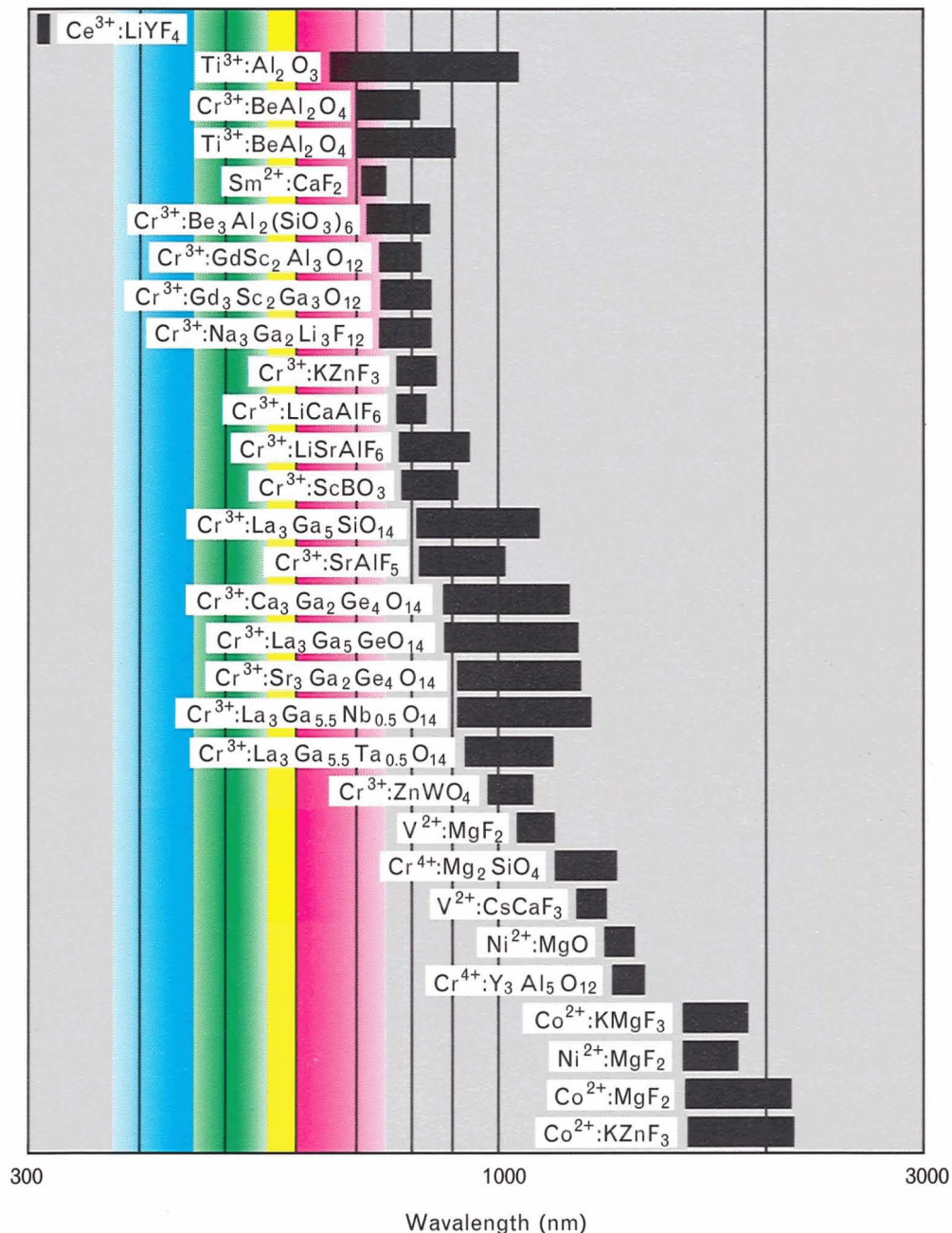


FIGURE 1. A representative list of tunable solid state lasers and their respective tuning ranges. This list shows that Ti:Al₂O₃ has the largest fractional tuning range, and that no tunable solid state laser has a tuning range that spans the visible region of the spectrum. The Cr³⁺ lasers account for over half of the lasers in this list.

strongly influenced by the crystal field. In tunable solid state lasers the interaction between the ion and the host crystal is such that lattice vibrations or phonons usually accompany the emission or absorption of photons. As a result the absorption and emission spectra become broadened in each laser. These *vibronic* transitions can provide gain over the large bandwidth required for tun-

able lasers. The rare-earth (Lanthanide ion) lasers, in which the outer electronic 5s, 5p, and 6s shells effectively shield the inner 4f electrons involved in the lasing transition, are generally not vibronic lasers and have relatively narrow bandwidths (as low as several cm⁻¹).

The broadband tunability of the Ti:Al₂O₃ laser provides beam-pointing agility in a laser radar by diffracting

the transmitted beam from a grating. Rapid tuning of the laser wavelength then causes rapid changes in the transmitted beam direction. An effort to develop a Ti:Al₂O₃ agile-beam laser radar was initiated at Lincoln Laboratory in 1985. To support a Ti:Al₂O₃ laser radar, advances were made in the growth of large Ti:Al₂O₃ crystals. These advances were soon followed by the development of a single-frequency, wavelength-agile, continuous-wave, room-temperature master oscillator (see the article by P.A. Schulz in this issue). A multistage pulsed amplifier was then developed to demonstrate the coherent laser radar requirements.

In this article we first discuss some of the details of the spectroscopy of Ti:Al₂O₃ and indicate how the coupling of the electronic energy levels of the Ti³⁺ ions to the phonons of the host sapphire crystal results in broad tunability. Next, we examine topics related to the growth of large high-quality Ti:Al₂O₃ crystals, and we describe our design and prototype of a tunable Ti:Al₂O₃ laser for an agile-beam optical radar. Finally, as an example of an application in which the properties of Ti:Al₂O₃ are particularly well suited, we briefly discuss the generation

and application of short pulses (approximately 100 fsec) with high peak intensities (greater than 10¹⁸ W/cm²).

Spectroscopy

In titanium-doped sapphire the titanium ions substitute for the aluminum ions and (when grown properly) exist in only the 3+ charge state. The energy levels of the titanium ions are particularly simple to analyze because only a single d electron is in the outermost shell while the remaining 18 electrons have the filled-shell configuration of a neutral argon atom. When the titanium ions are placed in a host crystal, the electrostatic field of neighboring atoms, or the *crystal field*, removes the five-fold angular momentum degeneracy of the single d electron.

In Ti:Al₂O₃ the 3d electron electrostatically interacts with the electronic charges of six surrounding oxygen ions that are positioned at the corners of an octahedron, as shown in Figure 2. In three of the the five angular momentum states of the 3d electron (designated as the triplet T), the orbitals do not point directly at the neighboring oxygen atoms; these states have lower ener-

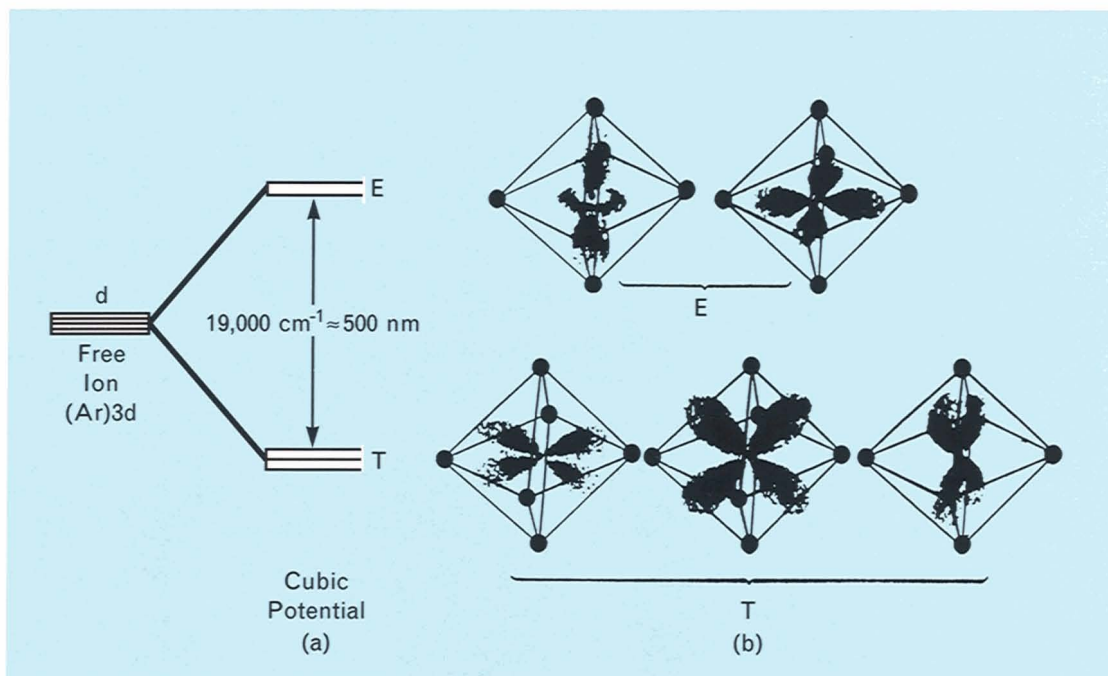


FIGURE 2. The left side of this figure shows a simplified energy-level diagram of Ti³⁺. The electronic configuration of the free ion is that of an argon shell plus a single 3d electron. The crystal field of the sapphire lattice removes the fivefold degeneracy of the ground-state level of the free ion to a triplet T ground state and a doublet E excited state. The right side of the figure shows the orientation of the 3d electronic orbitals with respect to the octahedrally coordinated nearest-neighbor oxygen atoms.

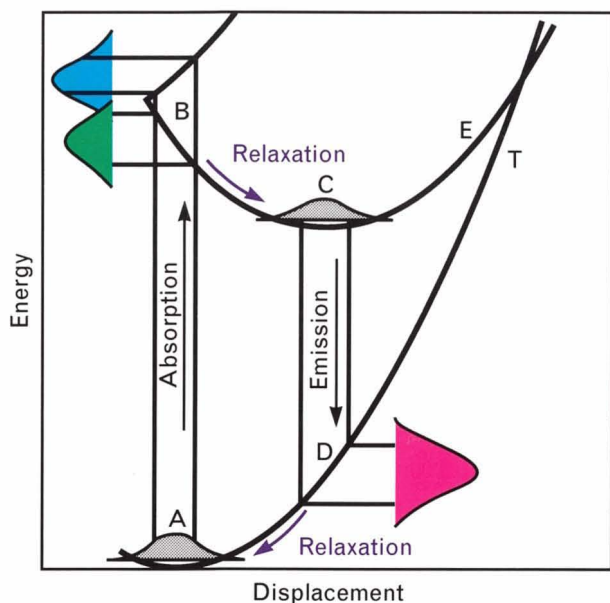


FIGURE 3. The Ti:Al₂O₃ configurational diagram. The energy of the electronic states are plotted with respect to the displacement of the Ti³⁺ ion. Absorption is indicated by the vertical transition from A to B and occurs in the blue and green region of the spectrum as indicated to the left. The emission of light is indicated by the transition from C to D and occurs in the red to infrared region of the spectrum as indicated at the right.

gy than the two states in which the orbitals point directly at the oxygen atoms (the doublet designated as E). This difference in energy corresponds to the energy of a green photon (approximately 500 nm or 19,000 cm⁻¹), and absorption of green light causes transitions from the ground state T to the excited state E. The same process occurs in octahedrally coordinated [Ti(H₂O)₆]³⁺ complexes, which also absorb in the green [12].

The electronic energy levels of the Ti³⁺ ions in Ti:Al₂O₃ are further perturbed by the sapphire host lattice. When the Ti³⁺ ion is in the excited state, the overall energy of the system can be lowered if the position of the Ti³⁺ ion displaces itself with respect to the surrounding oxygen atoms (the Jahn-Teller effect) [13]. This displacement removes the degeneracy of the two excited angular momentum states, which leads to a splitting of the green absorption band. Also, as the Ti³⁺ ion moves to its new equilibrium position, it kicks the surrounding lattice and excites vibrations (or phonons); this action is why the Ti:Al₂O₃ laser is called a vibronic laser.

The coupling of the electronic energy levels of the

Ti³⁺ ions with the vibrational energy levels of the surrounding sapphire lattice is essential for Ti:Al₂O₃ to operate as a laser. Figure 3 shows an energy-level diagram for Ti:Al₂O₃ in which the effects of phonon coupling are included. The abscissa represents the displacement of the Ti³⁺ ion. This energy-level diagram resembles that of a large polyatomic molecule such as an organic dye molecule. When the Ti³⁺ ion either absorbs or emits a photon, the 3d electron rearranges its orbital more quickly than the heavier Ti³⁺ nucleus can move (the Franck-Condon principle) [14]. Thus optical transitions are represented as vertical lines in the figure. The Gaussian-shaped curves at points A and C in the figure represent the probability of finding the Ti³⁺ at a particular position in the lowest vibrational state of the T and E levels, respectively.

Figure 3 shows absorption of light as the transition from point A to B. The transition is to either of the Jahn-Teller split upper states, and it results in a broad blue-green absorption, as shown in Figure 4. The Jahn-Teller splitting is not totally resolved and is manifested as a main peak with a shoulder. At point B in Figure 3 the ion displaces itself and lowers its energy by emitting phonons.

The transition from point C to point D shows the emission of light. Again the ion relaxes quickly to the ground state by emitting phonons. Two important results can be noted. First, the emission of light following the absorption of green light is at a longer wavelength (red, or Stokes shifted). A population inversion in the red emission band, necessary for amplification, is more easily achieved because the emission terminates on high vibrational levels of the ground state, which are unpopulated because of the fast vibrational relaxation rate. Second, a large emission bandwidth (and therefore broad tunability), as shown in Figure 4, results because the spread in probability of the Ti³⁺ ion position at the bottom of the E potential can connect via vertical transitions to a large spread of vibrational levels of the T potential. The width of the emission bandwidth depends on the details of the potential curves.

A final desirable feature that the Ti³⁺ energy levels exhibit is that further excited levels of the 3d electron lie far above the E levels. The Ti³⁺ ion exhibits no excited-state absorption (ESA); higher energy levels are far enough removed so that green light (pump photons) or red light

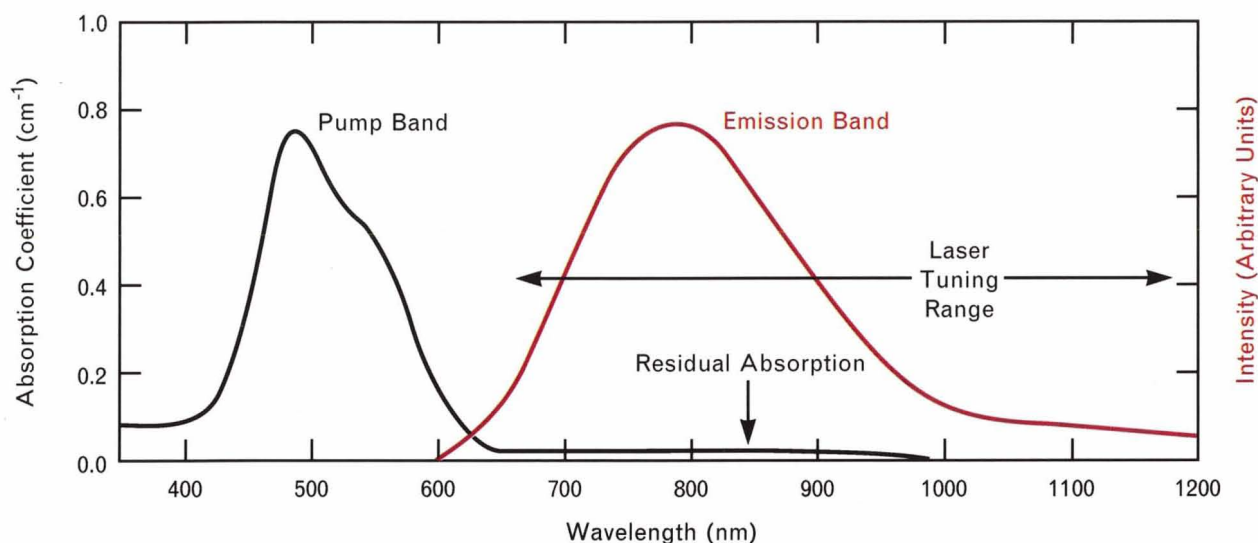


FIGURE 4. The emission and absorption bands of $\text{Ti:Al}_2\text{O}_3$. The absorption band, which peaks near 490 nm, occurs in the blue-green region of the spectrum and allows $\text{Ti:Al}_2\text{O}_3$ to be pumped by argon-ion lasers, frequency-doubled Nd:YAG lasers, copper-vapor lasers, or flashlamps. The emission band peaks near 790 nm. A weak absorption band that overlaps the emission band is known as the residual absorption.

(laser photons) cannot cause transitions from the E level to higher levels. The situation with other 3d transition metal ion lasers is more complex, and ESA is present to some degree.

The various lifetimes of the energy levels of a laser strongly influence laser operation by determining the dynamics of the population inversion. In a four-level laser the lower laser level must quickly relax to the ground state; otherwise a bottleneck occurs and the signal gain disappears. The spontaneous lifetime of the population in the upper laser level (the time in which $1/e$ of the population in the upper laser level decays to the lower laser level in the absence of a signal) is denoted by τ . This quantity determines the available time for the pump to create and store a population inversion. For $\text{Ti:Al}_2\text{O}_3$ at room temperature τ is 3.2 μsec . For comparison, τ is 230 μsec for Nd:YAG and 3 msec for ruby.

Another important parameter in the design and operation of a laser is the stimulated emission cross section (or gain cross section). This cross section, denoted as σ and measured in units of area, determines how many transitions from the upper to lower level are caused by a particular flux of photons. The gain per unit length of an amplifier is given by $N\sigma$, where N is the population inversion density. For a high-gain amplifier and a low-

threshold oscillator, a large value of σ is desirable. We can estimate σ for a material before laser-quality crystals are grown by performing spectroscopic measurements of the fluorescence profile Δf and the fluorescence lifetime τ . The emission cross section is given by

$$\sigma = \frac{3}{4\pi^2} \frac{\lambda^2}{n^2 \tau \Delta f}, \quad (1)$$

where λ is the peak of the fluorescence curve, n is the index of refraction, and Δf is the width (full width at half maximum) of the fluorescence curve in frequency [15]. From small-signal gain measurements in a $\text{Ti:Al}_2\text{O}_3$ amplifier we have determined the value of σ to be $3.0 \times 10^{-19} \text{ cm}^2$ [16].

The broad absorption band of $\text{Ti:Al}_2\text{O}_3$ allows it to be pumped by a variety of methods. Since the peak of the absorption is in the blue-green region of the spectrum, argon-ion lasers (which have strong laser lines at both 515 and 488 nm) can be used to pump continuous-wave $\text{Ti:Al}_2\text{O}_3$ lasers. Frequency-doubled Nd:YAG lasers, which emit in the green (532 nm), and copper-vapor lasers, which emit in the green (510 nm) and yellow (578 nm), can be used as efficient pumps for pulsed $\text{Ti:Al}_2\text{O}_3$ lasers. Flashlamp pumping of $\text{Ti:Al}_2\text{O}_3$ also was demonstrated, and 2% efficiency was achieved when fluorescent converters were used to shift some of

the broadband flashlamp emission that fell outside the absorption band back into the absorption band [17]. Although direct diode pumping of $\text{Ti}:\text{Al}_2\text{O}_3$ does not appear promising, recent advances in efficient diode-pumped Nd lasers indicate that an all-solid-state $\text{Ti}:\text{Al}_2\text{O}_3$ laser (both continuous wave and pulsed) will soon be a reality.

Crystal Growth and Material Characterization

Single crystals of $\text{Ti}:\text{Al}_2\text{O}_3$ used at Lincoln Laboratory in early laser experiments [2, 3] were grown by the Czochralski [18] and heat-exchanger [19] methods. A weak absorption band, as well as microscopic inhomogeneities such as bubbles or inclusions, limited the laser performance; modifications in the growth procedure, however, resulted in high-quality crystals that are now commercially available. To advance develop-

ment of the $\text{Ti}:\text{Al}_2\text{O}_3$ laser, Lincoln Laboratory researchers undertook a crystal growth effort that used the seeded vertical-gradient freeze method. This technique had been previously used to grow laser-quality $\text{Ni}^{2+}:\text{MgF}_2$ single crystals [20].

Figure 5 illustrates the vertical-gradient freeze growth technique [6]. A growth charge consisting of a mixture of sapphire crackle and single crystal pieces of Ti_2O_3 is prepared, and a tungsten crucible containing the sapphire seed and the charge is placed inside a furnace. The top and sides of the crucible are thermally insulated with molybdenum shields so that a vertical temperature gradient is established in the crucible. The furnace is heated in a vacuum until the charge is melted. Then the furnace is backfilled with helium, and gradually cooled to room temperature so that the charge solidifies from the bottom up. Most of the titanium is incorporated as Ti^{3+}

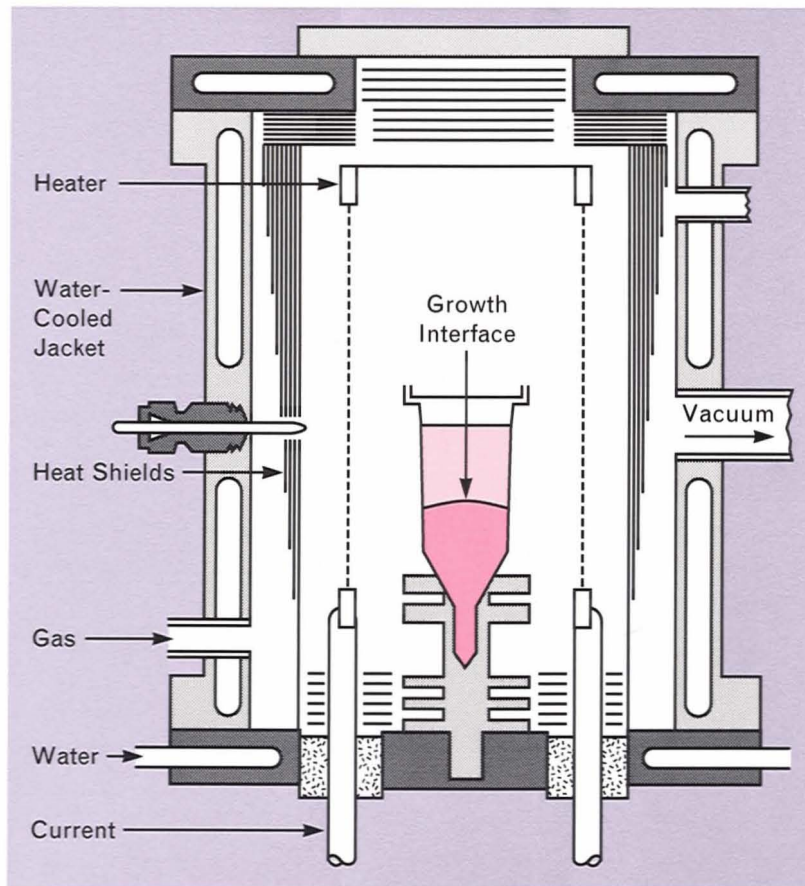


FIGURE 5. The apparatus for the vertical-gradient freeze crystal growth technique. The crystal, which is grown from the bottom up, starts at a seed at the base of the crucible. Tapered heat shields provide a vertical thermal gradient that causes the top of the crucible and melt to be hotter than the bottom.

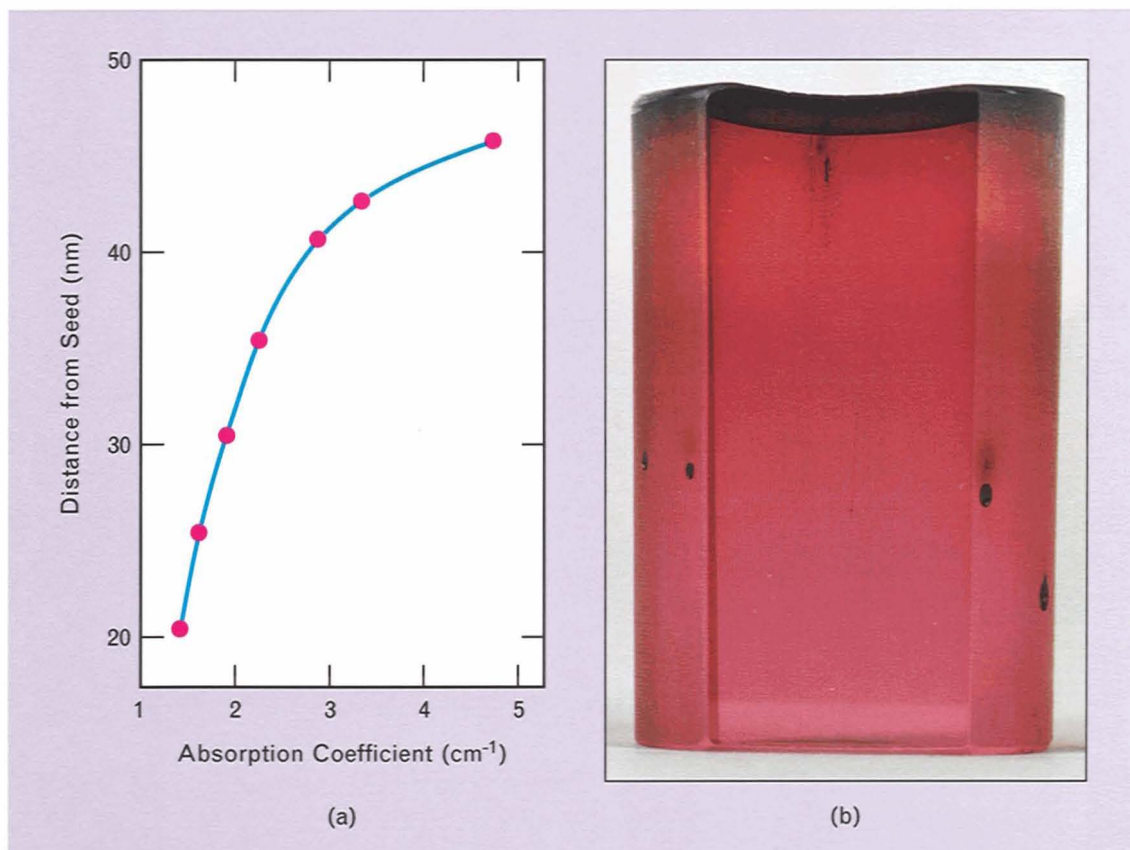


FIGURE 6. Absorption versus position in a Ti:Al₂O₃ crystal grown by the vertical-gradient freeze technique: (a) A plot of the absorption coefficient of a Ti:Al₂O₃ boule as a function of the vertical distance from the seed. (b) A photograph of a 2.5-cm diameter Ti:Al₂O₃ boule.

substituting for the Al³⁺ in the lattice. Because the distribution coefficient (the ratio of titanium concentration in the liquid and solid sides of the growth interface) is less than unity, the melt gets richer in titanium as the growth progresses. Figure 6 shows a 2.5-cm-diameter crystal grown by this technique; the crystal is darker at the top because of the higher titanium concentration. The highest absorption coefficient (at 490 nm, the peak of the absorption) measured near the top of the crystal was 5 cm⁻¹, which corresponds to a Ti₂O₃ concentration of 0.15 wt-%.

Present in the absorption spectrum shown in Figure 4 is a weak broad absorption peak that occurs in the region of laser emission. This absorption, although small, strongly influences the laser threshold (the pump power at which lasing begins) and the overall efficiency of continuous-wave lasers. This absorption is known as the *residual absorption*; its elimination was one of the major problems in the early development of Ti:Al₂O₃ crystals.

An experiment determined that if some of the Ti³⁺

ions were changed to Ti⁴⁺ by annealing the Ti:Al₂O₃ in an oxidizing atmosphere, the residual absorption would increase and reach a maximum at the point where 50% of the titanium ions were Ti³⁺ and 50% were Ti⁴⁺ [21]. Figure 7 shows the dependence of the residual absorption (at 780 nm) on the main absorption (at 490 nm). The main absorption is proportional to the concentration of Ti³⁺ ions. The parabolic dependence shown in the figure leads to the conclusion that the residual absorption is due to the presence of Ti³⁺-Ti⁴⁺ pairs. The amount of Ti⁴⁺, and therefore the number of Ti³⁺-Ti⁴⁺ pairs, present in a Ti:Al₂O₃ crystal can be minimized by growing the crystal in an oxygen-free atmosphere. The number of Ti⁴⁺ and Ti³⁺-Ti⁴⁺ pairs can be further decreased by postgrowth annealing in a reducing atmosphere such as hydrogen.

Tunable Ti:Al₂O₃ Laser for Agile-Beam Optical Radar

We will describe the design and prototype of a laser

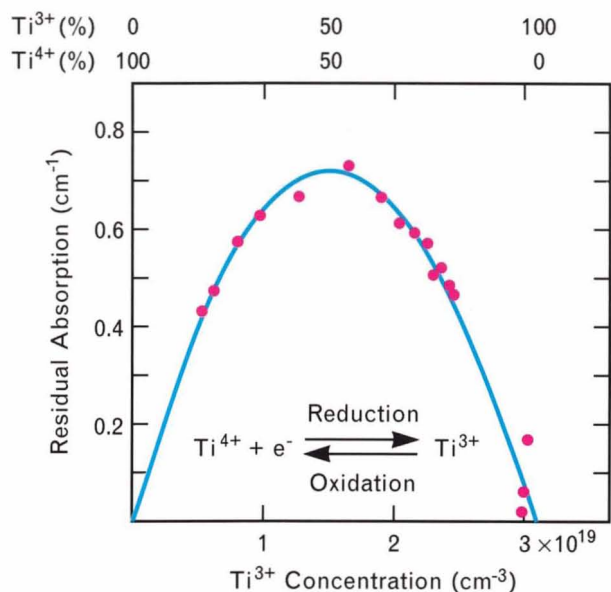


FIGURE 7. A plot of the peak residual absorption coefficient (at 780 nm) versus the main absorption coefficient (at 490 nm). To the left of the curve, corresponding to a main absorption equal to 0, all of the titanium ions are in the Ti^{4+} state. To the right of the curve, corresponding to a maximum main absorption, the titanium ions are in the Ti^{3+} state. At a point halfway between these two values the residual absorption is a maximum. This implies that the residual absorption is caused by Ti^{3+} - Ti^{4+} pairs.

radar transmitter as an example of the complex lasers that are being designed with $Ti:Al_2O_3$. Laser beam agility requirements can be significantly stressing in some radar applications. A possible approach to the design

problem uses the wavelength agility of a widely tunable solid state laser, such as $Ti:Al_2O_3$, to achieve beam agility. When the laser beam is diffracted from a grating, the pointing direction can be controlled in one dimension by the laser wavelength while a continuous mechanical scan can achieve two-dimensional coverage. In one scheme, shown in Figure 8, the entire platform rotates to provide the mechanical scan that (together with a radial wavelength scan) covers the field of view. A counterscanner that deflects the laser beam in a direction opposite to the mechanical motion of the platform is necessary to dwell on a target for the duration of a measurement; an acousto-optic deflector is a suitable counterscanner for the typically small angular deflections involved.

Figure 9 shows the block diagram for the laser transmitter in a master-oscillator/power-amplifier (MOPA) configuration. The $Ti:Al_2O_3$ master oscillator can be rapidly tuned from 700 to 900 nm by an electro-optic intracavity tuner. In addition, range-Doppler imaging requires frequency chirps (indicated in the figure by the dashed lines under the square amplitude pulse); these chirps are generated by an external single-sideband frequency modulator. Intracavity modulation techniques, which are possible because of the large bandwidth of the gain medium, can also be used to provide the required frequency chirps. The frequency-modulated pulse must then be amplified (these techniques are discussed below). The development of an efficient pump source for this amplifier is a major challenge. Several pumping schemes are possible; in Figure 9 the pump at 532 nm is

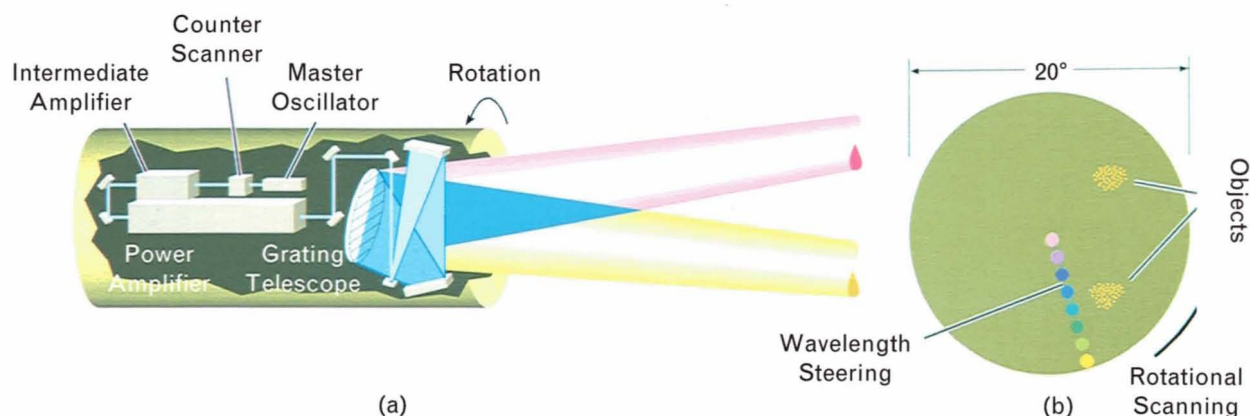


FIGURE 8. A conceptual picture of an agile-beam laser radar: (a) Rotation of the platform yields beam steering in an azimuthal direction while the combination of a frequency-agile laser and a diffraction grating provides beam steering in a radial direction. (b) A view of the target area.

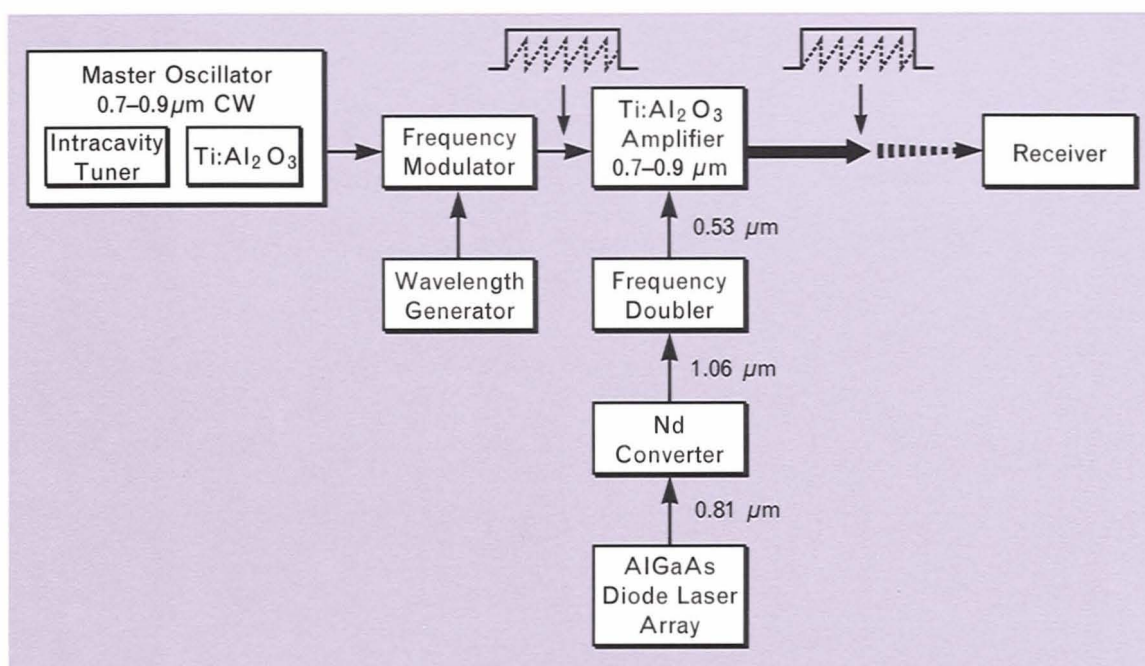


FIGURE 9. A simplified block diagram of a Ti:Al₂O₃ laser radar. In this proposed system the Ti:Al₂O₃ amplifier is pumped by an all-solid-state laser consisting of a diode-pumped frequency-doubled Nd:YAG laser. In our laboratory prototype the diode-pumped laser was replaced by a flashlamp-pumped system.

generated by many frequency-doubled Nd laser modules that in turn are diode pumped. We used a commercial flashlamp-pumped Nd:YAG laser, instead of a diode laser pump source, for our laboratory implementation of a Ti:Al₂O₃ amplifier at the 10-W average-power level, because the development of high-power diode-pumped Nd laser modules requires a substantial effort.

Because a laser oscillator with the desired characteristics is often difficult to scale to high powers, an MOPA architecture (in which an oscillator is amplified to the desired power level by a chain of amplifiers) was chosen. This architecture provides the flexibility to choose pulse lengths, and allows us to impose frequency chirps or other forms of frequency modulation on the transmitted radiation. In its basic form an MOPA consists of a master oscillator, which provides the signal beam, followed by a linear chain of amplifiers (in series, parallel, or a combination of both). The master oscillator can be either continuous wave or pulsed. In our design we chose a continuous-wave master oscillator to meet the frequency and coherence requirements of the laser radar.

The power-amplifier portion of the MOPA, which is divided into discreet sections separated by optical isolators, prevents parasitic oscillation and limits amplified

spontaneous emission. The design of a power amplifier requires knowledge of the damage threshold and the saturation fluence of the laser material $h\nu/\sigma$, where h is Planck's constant and ν is the frequency. The design of an efficient amplifier required a decision on the number of amplifier stages and the allocation of the available pump energy among the stages. For a continuous-wave laser amplifier a method exists that minimizes pump power by allocating it appropriately among the amplifier stages [22].

A large number of stages are required for simultaneous high efficiency and high gain. In the limit where the signal fluence is small compared to the saturation fluence of the material, the signal grows exponentially as it propagates through the medium. In this limit the signal does not appreciably disturb the excited-state population (which can be thought of as the stored pump energy), and little power transfer occurs between the pump and signal beams. In the limit where the signal beam is large compared to the saturation fluence, the signal grows linearly and the gain is said to saturate. The signal causes substantial amounts of stimulated emission and effectively transfers power from the pump to the signal beam. A typical MOPA begins with low-

efficiency high-gain stages and ends with high-efficiency low-gain stages.

In designing a linear chain of amplifiers, one must first decide what the largest small-signal gain or, equivalently, what the pump energy for each stage must be. The small-signal gain is determined by the damage threshold of the material for laser-pumped amplifiers or the available energy for flashlamp-pumped amplifiers. For Ti:Al₂O₃ the largest small-signal gain that is achievable in a single stage is approximately 4 cm⁻¹ [16]. In addition, the point at which the stage begins to exhibit parasitic oscillations also determines the pump energy. In many MOPA configurations the signal beam progressively increases in size as it propagates through the amplifier chain. There are two reasons for this increase. First, the signal-beam fluence increases as it propagates through the amplifier stages, and the signal beam is expanded to avoid damage to mirrors and other optical components. Second, for laser-pumped amplifiers, the latter stages (with more efficient energy extraction) are pumped with more energy than the first stages. To avoid damaging the laser crystals with the pump beams, the pump beams are made larger in size (the pump fluence is kept constant at 6.5 J/cm²). Since the signal beams are matched to the pump beams, the signal beam is also enlarged at the latter stages.

The longitudinally pumped multistage Ti:Al₂O₃ MOPA system that we constructed [23] has produced pulsed (10 Hz) tunable radiation from 760 to 825 nm. We obtained 100-nsec full-width at half-maximum single-frequency output with approximately 0.4 J/pulse at 800 nm [24]. The intensity profile of the output beam is elliptically Gaussian and is near diffraction limited (approximately 1.1 times the diffraction limit) [25]. The system is composed of three major subsystems: (1) a continuous-wave Ti:Al₂O₃ master oscillator, (2) a Ti:Al₂O₃ amplifier, and (3) frequency-doubled Nd:YAG pump lasers. Each of these subsystems is briefly described below.

The master oscillator is a continuous-wave Ti:Al₂O₃ single-frequency ring laser that is pumped by a continuous-wave argon-ion laser [26]. The Ti:Al₂O₃ ring laser can be tuned from 750 to 850 nm. The laser operates in a TEM₀₀ mode (the intensity profile can be described as a cylindrically symmetric Gaussian), and the frequency stability of the laser was measured as 2 MHz over a

10-sec time interval. At the peak of the gain profile the master oscillator provides a power of 0.5 W. A broadband isolator [27], consisting of a Faraday rotator and a compensating polarization rotator, provides the master oscillator with 30 dB of isolation from the amplifier chain over the tuning range of the master oscillator.

The Ti:Al₂O₃ amplifier consists of four stages: a four-pass preamplifier, a two-pass amplifier, a single-pass amplifier, and a final two-pass amplifier, as illustrated in Figure 10. A broadband isolator positioned between stages 1 and 2, and also between stages 2 and 3, prevents parasitic oscillation. Pockels cells between stages 1 and 2 are used to gate and temporally shape the signal-beam intensity. The frequency-doubled Nd:YAG pump lasers have a repetition rate of 10 Hz, which determines the pulse rate of the Ti:Al₂O₃ amplifier system. Figure 11 is a photograph of the multistage Ti:Al₂O₃ MOPA system.

Each amplifier stage consists of a Ti:Al₂O₃ crystal cut at Brewster's angle to minimize reflection losses. The signal and pump beams propagate almost colinearly (within 1°) and are polarized along the *c*-axis of the crystal (p polarization) to maximize the gain. The length of each crystal is chosen so that more than 95% of the pump beam is absorbed. Each stage is pumped from both sides to maximize the pump energy absorbed and to avoid damage to the Ti:Al₂O₃ crystals.

The preamplifier is pumped with a commercially available frequency-doubled Q-switched Nd:YAG laser. The power amplifier is pumped with a custom Nd:YAG laser that consists of a Q-switched mode-locked oscillator, a common three-stage amplifier chain, and four parallel two-stage power-amplifier chains, which results in four output beams at 1.06 μm. The repetition rate is 10 Hz. The total average power output of this laser at a wavelength of 1.06 μm was as high as 110 W.

Frequency doubling of the custom Nd:YAG laser from 1.06 to 0.532 μm was accomplished with KD*P doubling crystals. Doubling efficiency as high as 38% was achieved, and a doubling efficiency of 30% was achieved routinely. Because four separate laser beams are the output of the custom Nd:YAG laser, four separate frequency doublers were used, as shown in Figure 12. Transmissive random binary-phase plates were used to smooth out hot spots in the frequency-doubled beams [28].

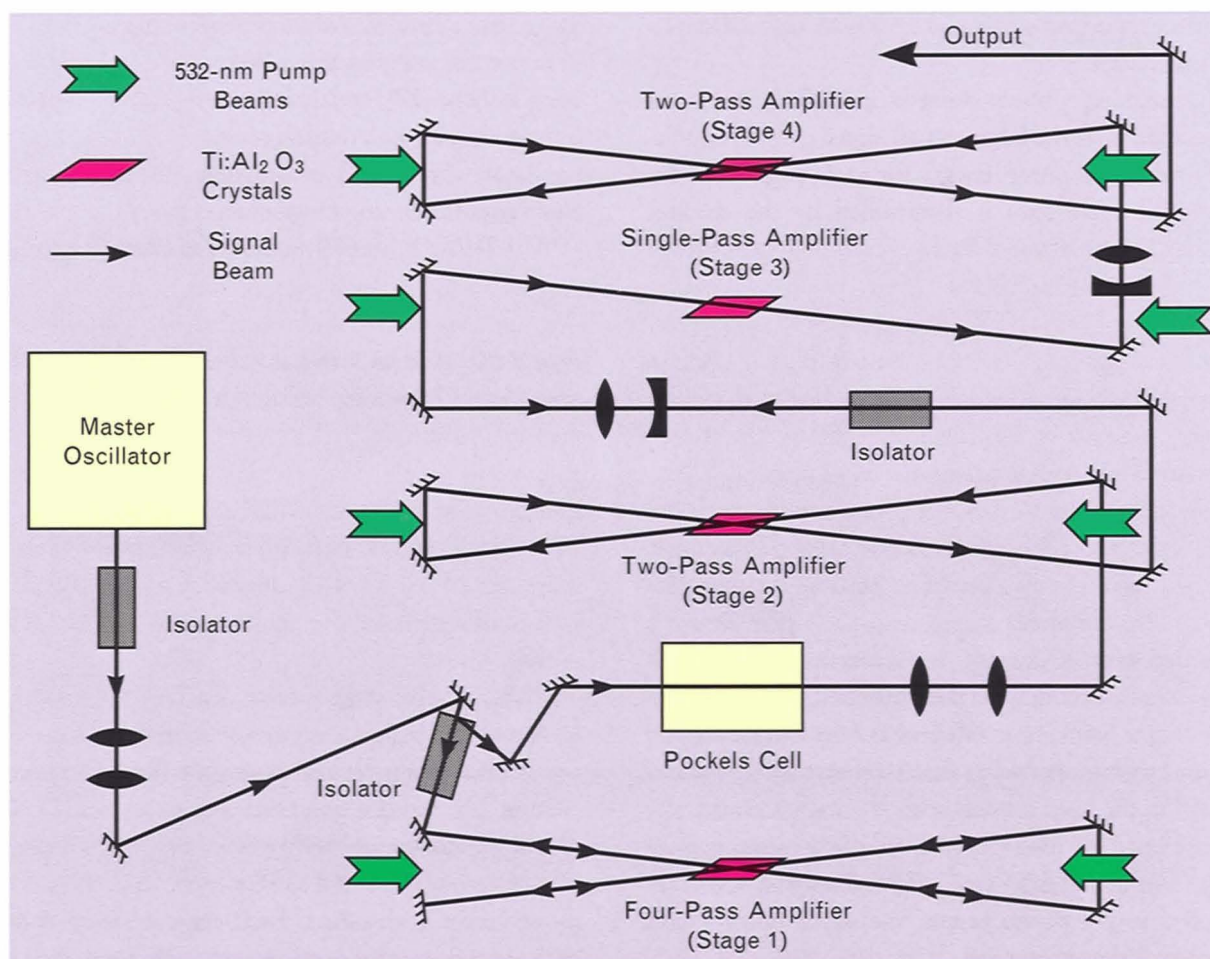


FIGURE 10. A diagram of the experimental setup of our laboratory prototype Ti:Al₂O₃ amplifier. Multipassing of the amplifiers is used extensively to increase the overall gain of the system. The Ti:Al₂O₃ amplifier crystals are pumped from both sides to increase the gain while minimizing the risk of damage to the crystals.

Amplification and Generation of Short Pulses

The generation and amplification of short pulses (less than 10^{-12} sec) is one area in which Ti:Al₂O₃ lasers are particularly well suited. The explanation of this ability is that all optical pulses are constrained by the uncertainty principle [29]

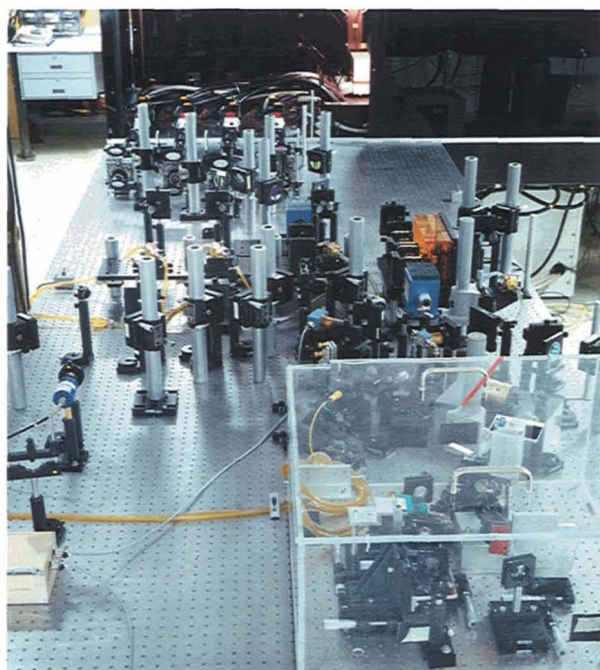
$$\Delta f_{rms} \Delta t_{rms} \geq \frac{1}{2}, \quad (2)$$

where Δf_{rms} and Δt_{rms} are root-mean-square widths of the pulse in frequency and time, respectively. Thus, to generate short pulses, a large-gain bandwidth must be available. For Ti:Al₂O₃, where Δf is approximately 2×10^{14} Hz, pulses as short as a few femtoseconds can be generated.

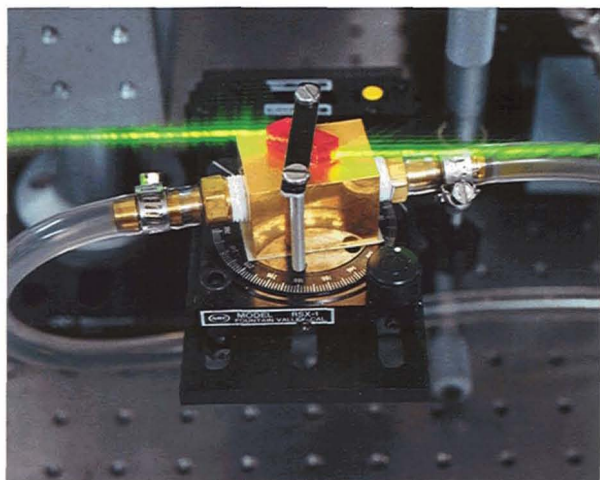
Several methods currently exist for generating short pulses by using Ti:Al₂O₃. Active mode locking by an

acousto-optic modulator has generated pulses as short as 1.3 psec [30]. A fiber-prism pulse compressor shortened these pulses to 50 fsec. Additive pulse mode-locking techniques have generated pulses that are 200 fsec in length [31]. Finally, 90-fsec pulses were spontaneously generated by a process known as self mode locking [32].

At intensities of 10^{18} W/cm² the interaction of light with matter begins to exhibit nonlinearities that are fundamentally different from the nonlinearities seen at lower intensities, such as frequency doubling and four-wave mixing. Because of its large bandwidth and high saturation fluence, Ti:Al₂O₃ can amplify pulses that are in the femtosecond domain to attain terrawatt and petawatt peak powers [33, 34]. The method of chirped-pulse amplification [35] (in which a femtosecond pulse is stretched temporally, given a linear chirp in the fre-



(a)



(b)

FIGURE 11. (a) A photograph of the prototype Ti:Al₂O₃ amplifier. In the foreground, within the plexiglass box, is the master oscillator. Farther back is the Ti:Al₂O₃ amplifier, followed by the frequency doublers for the Nd:YAG pump laser. (b) A Ti:Al₂O₃ amplifier crystal is pumped from both sides by the 532-nm pump beams.

quency domain, amplified, and temporally recompressed by a pair of gratings back to the femtosecond domain) avoids high peak powers (which can cause optical damage) within the amplifier stages. Other laser systems, such as excimer lasers or Nd:glass lasers, are capable of terra-

watt levels, but most systems do not offer the compactness associated with a solid state system.

A terrawatt laser system based upon Ti:Al₂O₃ can be a pump source for bench-top soft X-ray laser systems. Soft X-ray lasers use an intense pulse of light to vaporize a strip of metal such as selenium. A plasma is generated in which 24 of the 34 electrons in the selenium are stripped away. Energetic electrons collide with the selenium ions and excite 2p electrons to the 3p level. Lasing occurs between the 3p and 3s levels at a wavelength of 20 nm. X-ray lasers offer advancements in such diverse fields as biology, solid state physics, photolithography, and plasma physics [36, 37], but to date have only been produced with building-size lasers as a pump source, such as the Nova facility at Lawrence Livermore Laboratory. The possibility of holographically imaging the three-dimensional structure of proteins and other key building blocks of life has spurred interest in X-ray lasers and the simultaneous development of pump sources such as Ti:Al₂O₃.

Another application of a Ti:Al₂O₃-based petawatt (greater than 10¹⁵ W) laser system is in the production of plasma waves to generate intense electric fields used in novel particle accelerators [38, 36]. Conventional particle accelerators can provide a maximum accelerating field of 1 MeV/cm⁻¹ before the accelerator walls begin to break down. The size of the accelerator is scaled to the energies at which particles can be accelerated; this fact leads to proposed machines such as the superconducting supercollider with a circumference of 87 km. One method of generating plasma waves, known as the beat-wave method, uses intense laser pulses of slightly different frequencies focused into a plasma. If the beat (or difference) frequency of the lasers corresponds to the plasma's natural resonance frequency, plasma waves are generated. Just as water waves accelerate surfboard riders, the intense electric fields associated with the plasma waves can accelerate particles. Studies show that the laser pulses must be temporally short (less than 100 psec) to prevent plasma instabilities from occurring. The accelerating potential theoretically possible with such a scheme is 1 GeV/cm⁻¹, which is three orders of magnitude higher than the potential that can be produced by conventional technology. For a KrF excimer-laser-based system, electrons could be accelerated to 10 Tev in 1 km [36], which is about two orders of magnitude smaller

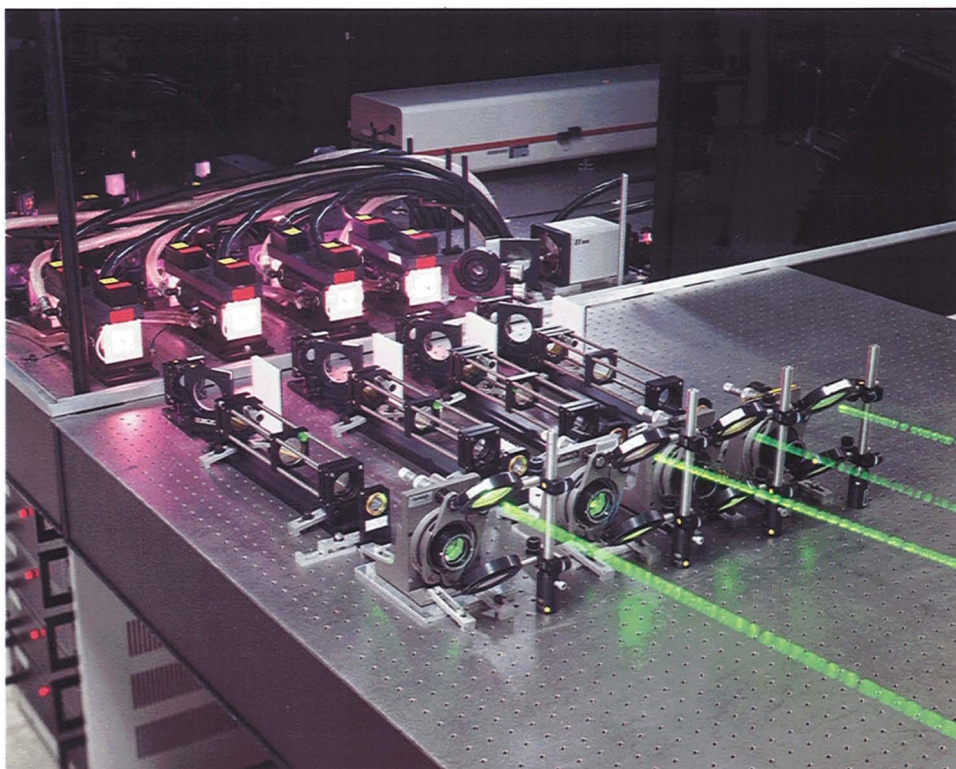


FIGURE 12. Frequency-doubling arrangement for the Nd:YAG pump laser. The crystal used for frequency doubling was KD*P. We routinely achieved 30% conversion efficiency for a total of 30 to 35 W of 532-nm radiation.

than the superconducting supercollider. $\text{Ti:Al}_2\text{O}_3$ could also provide a compact source for the laser beams in such future particle accelerators.

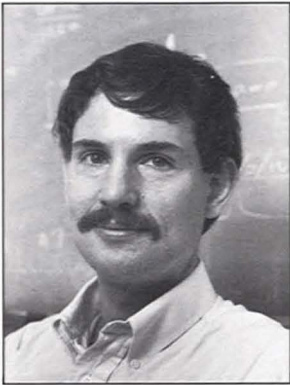
Acknowledgments

The authors gratefully acknowledge our collaborators in the development of the $\text{Ti:Al}_2\text{O}_3$ laser and amplifier: R.L.

Aggarwal, P.A. Schulz, P. Lacovara, V. Daneu, A. Walther, and R. Tapper. We also would like to thank R. Fahey and A.J. Strauss for growing $\text{Ti:Al}_2\text{O}_3$ crystals and providing them to us. We are grateful to M. Geis for providing us with the random binary-phase plates. Finally, we would like to thank P.L. Kelley, A. Mooradian, and I. Melngailis for their support and encouragement.

REFERENCES

1. T.H. Maiman, "Stimulated Optical Radiation in Ruby," *Nature* **187**, 493 (1960).
2. P.F. Moulton, "Ti-doped Sapphire Tunable Solid State Laser," *Opt. News* **8**, 9 (Nov./Dec. 1982).
3. P.F. Moulton, "Spectroscopic and Laser Characteristics of Ti:Al₂O₃," *J. Opt. Soc. Am. B* **3**, 125 (1986).
4. P. Albers, E. Stark, and G. Huber, "Continuous-Wave Laser Operation and Quantum Efficiency of Titanium-Doped Sapphire," *J. Opt. Soc. Am. B* **3**, 134 (1986).
5. A. Sanchez, R.E. Fahey, A.J. Strauss, and R.L. Aggarwal, "Room-Temperature Continuous-Wave Operation of a Ti:Al₂O₃ Laser," *Opt. Lett.* **11**, 363 (1986).
6. R.E. Fahey, A.J. Strauss, A. Sanchez, and R.L. Aggarwal, "Growth of Laser-Quality Ti:Al₂O₃ Crystals by a Seeded Gradient-Freezing Technique," in *Tunable Solid-State Lasers II*, eds. A.B. Budgor, L. Esterowitz, and L.G. DeShazer (Springer-Verlag, New York, 1986), p. 82.
7. W.R. Rapoport and C.P. Khattak, "Efficient, Tunable Ti:sapphire Laser," in *Tunable Solid-State Lasers II*, eds. A.B. Budgor, L. Esterowitz, and L.G. DeShazer (Springer-Verlag, New York, 1986), p. 212.
8. L.F. Johnson, R.E. Dietz, and H.J. Guggenheim, "Optical Maser Oscillation from Ni²⁺ in MgF₂ Involving Simultaneous Emission of Phonons," *Phys. Rev. Lett.* **11**, 318 (1963).
9. P.P. Sorokin and J.R. Lankard, "Stimulated Emission Observed from an Organic Dye, Chloro-Aluminum Phthalocyanine," *IBM J. Res. Dev.* **10**, 162 (1966).
10. F.P. Schäfer, W. Schmidt, and J. Volze, "Organic Dye Solution Laser," *App. Phys. Lett.* **9**, 306 (1966).
11. J.C. Walling, H.P. Jenssen, R.C. Morris, E.W. O'Dell, and O.G. Peterson, "Tunable-Laser Performance in BeAl₂O₄:Cr³⁺," *Opt. Lett.* **4**, 182 (1979).
12. P.W. Atkins, *Physical Chemistry* (W.H. Freeman, San Francisco, 1978), p. 490.
13. A. Abragam and B. Bleaney, *Electron Paramagnetic Resonance of Transition Ions* (Dover, New York, 1986), p. 790.
14. G. Herzberg, *Molecular Spectra and Molecular Structure III: Electronic Spectra of Polyatomic Molecules* (Van Nostrand Reinhold, New York, 1966), p. 8.
15. A.E. Siegman, *An Introduction to Lasers and Masers* (McGraw-Hill, New York, 1971), p. 402.
16. K.F. Wall, R.L. Aggarwal, R.E. Fahey, and A.J. Strauss, "Small-Signal Gain Measurements in a Ti:Al₂O₃ Amplifier," *IEEE J. Quantum Electron.* **QE-24**, 1016 (1988).
17. E.G. Erickson, "Flashlamp-Pumped Titanium:Sapphire Laser," *OSA Proc. on Tunable Solid State Lasers, Vol. 5*, eds. M.L. Shand and H.P. Jenssen (Optical Society of America, Washington, 1989), p. 26.
18. M. Kokta, "Growth of Titanium-Doped Sapphire," *Topical Mtg. on Tunable Solid-State Lasers* (Optical Society of America, Washington, 1985), p. ThB4.
19. F. Schmid and C.P. Khattak, "Growth of Co:MgF₂ and Ti:Al₂O₃ Crystals for Solid State Laser Applications," in *Tunable Solid State Lasers*, eds. P. Hammerling, A.B. Budgor, and A. Pinto (Springer-Verlag, New York, 1985), p. 122.
20. T.B. Reed, R.E. Fahey, and P.F. Moulton, "Growth of Ni-Doped MgF₂ Crystals in Self-Sealing Graphite Crucibles," *J. Crystal Growth* **42**, 569 (1977).
21. R.L. Aggarwal, A. Sanchez, M.M. Stuppi, R.E. Fahey, A.J. Strauss, W.R. Rapoport, and C.P. Khattak, "Residual Infrared Absorption in As-Grown and Annealed Crystals of Ti:Al₂O₃," *IEEE J. Quantum Electron.* **QE-24**, 1003 (1988).
22. A. Walther and A. Sanchez, "Pump Power Minimization for High Gain CW Laser Amplifiers," *App. Opt.* **27**, 828 (1988).
23. K.F. Wall, P.A. Schulz, R.L. Aggarwal, P. Lacovara, A. Walther, V. Daneu, and A. Sanchez, "Ti:Al₂O₃ Master-Oscillator/Power-Amplifier System," *Solid State Research Report*, Lincoln Laboratory (1990:1), p. 9.
24. K.F. Wall, P.A. Schulz, R.L. Aggarwal, P. Lacovara, A. Walther, V. Daneu, and A. Sanchez, "Temporal, Spectral, and Coherence Properties of a Ti:Al₂O₃ Master-Oscillator/Power-Amplifier," to be published in *Solid State Research Report*, Lincoln Laboratory.
25. K.F. Wall, P.A. Schulz, R.L. Aggarwal, P. Lacovara, A. Walther, V. Daneu, and A. Sanchez, "Beam Quality of a Ti:Al₂O₃ Master-Oscillator/Power-Amplifier System," *Solid State Research Report*, Lincoln Laboratory (1990:2), p. 11.
26. P.A. Schulz, "Single-Frequency Ti:Al₂O₃ Ring Laser," *IEEE J. Quantum Electron.* **24**, 1039 (1988).
27. P.A. Schulz, "Wavelength Independent Faraday Isolator," *App. Opt.* **28**, 4458 (1989).
28. P. Lacovara, K.F. Wall, R.L. Aggarwal, M. Geis, K. Krohn, and B.J. Felton, "Laser Pumping of Solid-State Amplifiers Using Random Binary-Phase Plates," *Solid State Research Report*, Lincoln Laboratory (1989:3), p. 10.
29. A.E. Siegman, *Lasers* (University Science Books, Mill Valley, CA, 1986), p. 334.
30. J.D. Kafka, M.L. Watts, D.J. Roach, M.S. Keirstead, H.W. Schaaf, and T. Baer, "Pulse Compression of a Mode-Locked Ti:Sapphire Laser," Postdeadline paper, *CLEO '90, Anaheim, CA, 21-25 May 1990*, CPDP8.
31. J. Goodberlet, J. Wang, J.G. Fujimoto, and P.A. Schulz, "Femtosecond Passively Mode-Locked Ti:Al₂O₃ Laser with a Nonlinear External Cavity," *Opt. Lett.* **14**, 1125 (1989).
32. D.E. Spence, P.E. Kean, and W. Sibbett, "Sub-100fs Pulse Generation from a Self-Modelocked Titanium-Sapphire Laser," Postdeadline paper, *CLEO '90, Anaheim, CA, 21-25 May 1990*, CPDP10.
33. H.C. Kapteyn, A. Sullivan, H. Hamster, and R.W. Falcone, "Multiterawatt Femtosecond Laser Based on Ti:Sapphire," in *Femtosecond to Nanosecond High-Intensity Lasers and Applications*, ed. E.M. Campbell, *Proc. SPIE* **1229**, 75 (1990).
34. D.J. Harter, M. Pessot, J.A. Squier, J. Nees, P. Bado, and G. Mourou, "Short Pulse Amplification in Tunable Solid State Materials," in *Femtosecond to Nanosecond High-Intensity Lasers and Applications*, ed. E.M. Campbell, *Proc. SPIE* **1229**, 19 (1990).
35. P. Maine, D. Strickland, P. Bado, M. Pessot, and G. Mourou, "Generation of Ultrahigh Peak Power Pulses by Chirped Pulse Amplification," *IEEE J. Quantum Electron.* **QE-24**, 398 (1988).
36. A.A. Hauer, D.W. Forslund, C.J. McKinstrie, J.S. Wark, P.J. Hargis Jr., R.A. Hamil, and J.M. Kindel, "Current New Applications of Laser Plasmas," in *Laser-Induced Plasmas and Applications*, eds. L.J. Radziemski and D.A. Cremers (Marcel Dekker, New York, 1989), p. 385.
37. D.L. Matthews and M.D. Rosen, "Soft X-Ray Lasers," *Sci. Am.* **259**, 86 (Dec. 1988).
38. J.M. Dawson, "Plasma Particle Accelerators," *Sci. Am.* **260**, 54 (Mar. 1989).



KEVIN F. WALL is a staff member in the Quantum Electronics Group. He received a B.S. in physics from Worcester Polytechnic Institute in 1976, an M.S. in physics from Rensselaer Polytechnic Institute in 1980, and a Ph.D. in applied physics from Yale University in 1986. From 1979 to 1980 he was employed at the General Electric Research and Development Center in Schenectady, N.Y., where he conducted research on Mossbauer studies of amorphous magnetic materials. Kevin joined Lincoln Laboratory in 1986, and his research is currently directed toward the development of tunable solid state lasers. He is a member of Sigma Xi and the Optical Society of America.



ANTONIO SANCHEZ is an assistant leader in the Quantum Electronics Group. He received the degree of Licenciado in physics from the University of Madrid in 1967 and a Ph.D. from MIT in 1973. He was a research associate in the Department of Physics at MIT before joining Lincoln Laboratory in 1977. His research includes the development of electron-beam-pumped semiconductor lasers, tunable solid state lasers, and diode-pumped solid state lasers. Dr. Sanchez is a member of the IEEE and the Optical Society of America.